Article

Defucosylated Monoclonal Antibody (H_2Mab-139-mG_{2a}-f) Exerted Antitumor Activities in Mouse Xenograft Models of Breast Cancers against Human Epidermal Growth Factor Receptor 2

Hiroyuki Suzuki [1,2,*,†], Tomokazu Ohishi [3,4,†], Ren Nanamiya [1], Manabu Kawada [4], Mika K. Kaneko [1,2] and Yukinari Kato [1,2,*]

[1] Department of Molecular Pharmacology, Tohoku University Graduate School of Medicine, 2-1 Seiryo-machi, Aoba-ku, Sendai 980-8575, Miyagi, Japan; ren.nanamiya.p5@dc.tohoku.ac.jp (R.N.); k.mika@med.tohoku.ac.jp (M.K.K.)

[2] Department of Antibody Drug Development, Tohoku University Graduate School of Medicine, 2-1 Seiryo-machi, Aoba-ku, Sendai 980-8575, Miyagi, Japan

[3] Institute of Microbial Chemistry (BIKAKEN), Numazu, Microbial Chemistry Research Foundation, 18-24 Miyamoto, Numazu-shi 410-0301, Japan; ohishit@bikaken.or.jp

[4] Institute of Microbial Chemistry (BIKAKEN), Laboratory of Oncology, Microbial Chemistry Research Foundation, 3-14-23 Kamiosaki, Shinagawa-ku 141-0021, Tokyo, Japan; kawadam@bikaken.or.jp

* Correspondence: hiroyuki.suzuki.b4@tohoku.ac.jp (H.S.); yukinari.kato.e6@tohoku.ac.jp (Y.K.); Tel.: +81-22-717-8207 (H.S. & Y.K.)

† Contributed equally to this work.

Simple Summary: The clinically approved human epidermal growth factor receptor 2 (HER2)-targeting monoclonal antibodies (mAbs), trastuzumab and pertuzumab, target domains IV and II, respectively. Trastuzumab has become the standard treatment for HER2-overexpressed breast and gastric cancers, and trastuzumab in combination with pertuzumab showed clinical benefit. However, there still exist patients who do not respond to the therapy. Furthermore, HER2 mutants that cannot be recognized by pertuzumab were found in tumors. Therefore, novel anti-HER2 mAbs and modalities have been desired. We developed and evaluated a defucosylated anti-HER2 domain I mAb, H_2Mab-139-mG_{2a}-f, for its antibody-dependent cellular cytotoxicity (ADCC) *in vitro* and antitumor activity in mouse xenograft models. H_2Mab-139-mG_{2a}-f exhibited antitumor activities against HER2-positive BT-474, but not HER2-negative MDA-MB-468 xenograft-bearing mice.

Abstract: Two monoclonal antibodies (mAbs) against human epidermal growth factor receptor 2 (HER2), trastuzumab and pertuzumab, were clinically approved. We previously developed a highly sensitive and specific anti-HER2 mAb, H_2Mab-139 (mouse IgG_1, kappa). In this study, we produced a defucosylated IgG_{2a} version of anti-HER2 mAb (H_2Mab-139-mG_{2a}-f) to enhance ADCC-mediated antitumor activity. H_2Mab-139-mG_{2a}-f exhibits a high binding affinity in flow cytometry with the dissociation constant (K_D) determined to be 3.9×10^{-9} M and 7.7×10^{-9} M against HER2-overexpressed Chinese hamster ovary (CHO)-K1 (CHO/HER2) and HER2-positive BT-474 cells, respectively. Moreover, we showed that H_2Mab-139-mG_{2a}-f exerted ADCC and complement-dependent cytotoxicity against CHO/HER2 and BT-474 cells *in vitro* and exhibited potent antitumor activities in the xenograft models. These results indicated that H_2Mab-139-mG_{2a}-f exerts antitumor effects against HER2-positive human breast cancers and could be useful for an antibody treatment regimen for HER2-positive human cancers.

Keywords: HER2; breast cancer; monoclonal antibody; antitumor activities; mouse xenograft model; antibody-dependent cellular cytotoxicity

 doi:10.20944/preprints202307.0169.v1

1. Introduction

Human epidermal growth factor receptor 2 (HER2) is included in the receptor tyrosine kinase family of human epidermal growth factor receptor (EGFR). The HER activation is controlled by EGF-family ligands under physiological conditions. The formation of multiple combinations of HER homo- and heterodimers is induced by ligand binding, which triggers the activation of the cytoplasmic tyrosine kinase domain. The activation of several downstream signaling pathways, such as the RAS/RAF/MAPK and PI3K/AKT pathways [1] were induced by the autophosphorylation of specific tyrosine residues. HER2 does not have ligands and cannot form ligand-dependent homodimers, unlike EGFR, HER3, and HER4. To activate the downstream signaling, HER2 must either form heterodimers with other HER members and their specific ligands or self-assemble into ligand-independent homodimers when overexpressed. HER2 possesses four extracellular domains (I–IV) [2]. The domain II is known to be essential for the heterodimer formation with other HER members, such as EGFR, HER3, and HER4 in the presence of their ligands, such as EGF [3] and neuregulin 1 (NRG1, a HER3 ligand) [4].

HER2 is overexpressed in approximately 18% of breast cancers and is associated with higher rates of recurrence, poor prognosis, and shorter overall survival [5]. HER2 overexpression is also observed in ~20% of gastric cancers [6]. A monoclonal antibody (mAb) against domain IV of HER2, trastuzumab, exhibited an anti-proliferating effect *in vitro* and a potent antitumor effect *in vivo* [7,8]. The addition of trastuzumab to chemotherapy improves objective response rates, progression-free survival, and overall survival in HER2-positive breast cancer patients with metastasis [9]. Trastuzumab has become the standard treatment for HER2-positive breast cancers [10] and HER2-positive gastric cancers [11]. For more than 20 years, trastuzumab has been the most effective therapy for HER2-positive breast cancer [12].

Clinically, the efficacy of trastuzumab involves immunologic engagement [8]. The Fc domain of trastuzumab mediates engagement with Fcγ receptors (FcγRs) on various immune cells. The binding of trastuzumab to FcγR facilitates the phagocytosis of antibody-bound tumor cells, a process known as antibody-dependent cellular phagocytosis (ADCP). The FcγR engagement also activates dendritic cells, macrophages, and neutrophils, which can change adaptive immune responses through cytokine production, chemotaxis, and antigen presentation. Furthermore, the FcγR engagement mediates the activation of natural killer (NK) cells which attack and lyse the target tumor cells, termed antibody-dependent cellular cytotoxicity (ADCC) [13]. To improve the FcγRIIIA engagement and ADCC activity, margetuximab was developed by introducing several optimization mutations of trastuzumab [14]. Margetuximab was approved by U.S. Food and Drug Administration (FDA) and showed significant improvement in progression-free survival in heavily pretreated patients [15,16]. Moreover, the Fc domain of these mAbs can exert complement-dependent cytotoxicity (CDC) [17,18].

Another clinically approved HER2-targeting mAb, pertuzumab, binds to the domain II and prevents NRG1-induced heterodimerization with HER3 and intracellular signaling [19]. The heterodimerization is known to be an important mechanism for resistance to trastuzumab [19]. Therefore, pertuzumab is considered to possess a complementary mechanism to trastuzumab [20]. The first-line treatment combining trastuzumab, pertuzumab, and chemotherapy has been evaluated and demonstrated clinical benefits [21]. The double anti-HER2 blockade has been the standard therapy in the initial management of metastatic HER2-positive breast cancer [9]. However, HER2 (S310F/Y) is the most frequent oncogenic missense mutation which cannot be recognized by pertuzumab [22].

In our previous studies, we established several anti-HER2 mAbs, including H2Mab-77 (IgG_1, kappa) [23], H2Mab-119 (IgG_1, kappa) [24], and H2Mab-139 (IgG_1, kappa) [25] by the immunization of HER2 ectodomain. Those mAbs have been revealed to recognize the domain I of HER2, and are available for flow cytometry, western blotting, and immunohistochemistry (IHC) [23–25]. We have demonstrated that class-switched (from IgG_1 to IgG_{2a}) and defucosylated mAbs exert potent antitumor effects in several mouse xenograft models [26–33]. The defucosylated recombinant mAbs can be produced using fucosyltransferase 8 (FUT8)-knockout Expi-CHO-S cells [34].

In this study, we produced a defucosylated IgG_{2a} type of anti-HER2 mAb (H_2Mab-139-mG_{2a}-f), and evaluated the ability to induce ADCC and CDC *in vitro* or antitumor efficacy *in vivo* against HER2-positive and HER2-negative breast cancer cells.

2. Materials and Methods

2.1. Cell Lines

Chinese hamster ovary (CHO)-K1, LN229, BT-474, and MDA-MB-468 cell lines were obtained from the American Type Culture Collection (ATCC, Manassas, VA, USA). LN229/HER2 and CHO/HER2 were established by transfecting pCAG/PA-HER2-RAP-MAP into LN229 and CHO-K1 cells using Neon transfection system [Thermo Fisher Scientific, Inc. (Thermo), Waltham, MA] and Lipofectamine LTX (Thermo), respectively. A few days after transfection, PA tag-positive cells were sorted by a cell sorter (SH800; Sony Corp., Tokyo, Japan) using NZ-1, which was originally developed as an anti-human podoplanin (PDPN) mAb [35–49].

CHO-K1 and CHO/HER2 cell lines were cultured in Roswell Park Memorial Institute（RPMI）-1640 medium [Nacalai Tesque, Inc. (Nacalai), Kyoto, Japan]. LN229, BT-474, and MDA-MB-468 cell lines were cultured in DMEM medium (Nacalai). Both media were supplemented with 10% heat-inactivated fetal bovine serum (FBS; Thermo), 1 mM of sodium pyruvate, 100 units/ml of penicillin, 100 μg/ml streptomycin, and 0.25 μg/ml amphotericin B (Nacalai). All cell lines were cultured at 37°C in a humidified atmosphere with 5% CO_2 and 95% air.

2.2. Recombinant mAb Production

Anti-HER2 mAb H_2Mab-139 was established as previously described [25]. To generate H_2Mab-139-mG_{2a}-f, we subcloned V_H cDNA of H_2Mab-139 and C_H of mouse IgG_{2a} into the pCAG-Ble vector ［FUJIFILM Wako Pure Chemical Corporation (Wako), Osaka, Japan]. V_L cDNA of H_2Mab-139 and C_L cDNA of mouse kappa light chain were also subcloned into the pCAG-Neo vector (Wako). The vectors for the recombinant H_2Mab-139 were transduced into BINDS-09 (FUT8-knockout ExpiCHO-S) cells using the ExpiCHO Expression System (Thermo) [50]. H_2Mab-139-mG_{2a}-f was purified using Ab-Capcher (ProteNova Co., Ltd.).

2.3. Animal Experiments for ADCC Assay and Mice Xenograft Model

All Animal experiments for ADCC and antitumor activity of H_2Mab-139-mG_{2a}-f were approved (approval no. 2022-056, 2023-001, and 2023-018) by the Institutional Committee for Experiments of the Institute of Microbial Chemistry (Numazu, Japan). Mice were maintained and monitored as described previously [50]. The loss of original body weight was determined to a point >25% and/or a maximum tumor size >3,000 mm^3 as humane endpoints for euthanasia.

2.4. Flow Cytometry

CHO-K1, CHO/HER2, LN229, LN229/HER2, BT-474, and MDA-MB-468 cells were collected using 0.25% trypsin and 1 mM ethylenediamine tetraacetic acid (EDTA; Nacalai). The cells were treated with H_2Mab-139-mG_{2a}-f or blocking buffer (control) (0.1% BSA in PBS) for 30 min at 4°C. Then, the cells (1×10^5 cells/sample) were treated with Alexa Fluor 488-conjugated anti-mouse IgG (1:2,000; Cell Signaling Technology, Inc., Danvers, MA, USA) for 30 min at 4°C. To confirm the isotype of H_2Mab-139-mG_{2a}-f, the mAb-treated LN229/HER2 cells were incubated with Alexa Fluor 488-conjugated anti-mouse immunoglobulins, Fluorescein-conjugated anti-mouse heavy chains (IgG_1 and IgG_{2a}; SouthernBiotech, Birmingham, AL, USA). The fluorescence data were collected using SA3800 Cell Analyzer (Sony Corp.) and analyzed using FlowJo [BD Biosciences (BD), Franklin Lakes, NJ, USA].

Preprints (www.preprints.org) | NOT PEER-REVIEWED | Posted: 4 July 2023 doi:10.20944/preprints202307.0169.v1

2.5. Determination of Dissociation Constant (K_D) via Flow Cytometry

CHO/HER2 or BT-474 cells were suspended in 100 µl of serially diluted H_2Mab-139-mG_{2a}-f (600 pg/ml–10 µg/ml) followed by Alexa Fluor 488-conjugated anti-mouse IgG at a ratio of 1:200 (n = 3). Fluorescence data were collected using the SA3800 Cell Analyzer. The dissociation constant (K_D) was calculated by fitting binding isotherms to built-in one-site binding models in GraphPad Prism 8 (GraphPad Software, Inc., La Jolla, CA).

2.6. Western Blot Analysis

The cell lysates (10 µg) were boiled in sodium dodecyl sulfate (SDS) sample buffer (Nacalai) and separated on 5%–20% polyacrylamide gels (Wako). The proteins were transferred onto polyvinylidene difluoride membranes (Merck KGaA, Darmstadt, Germany). After blocking with 4% skim milk (Nacalai) in PBS with 0.05% Tween 20, The membranes were treated with 1 µg/mL of H_2Mab-139-mG_{2a}-f or 1 µg/mL of an anti-isocitrate dehydrogenase 1 (IDH1) mAb (clone RcMab-1) [51,52]. The membranes were then incubated with peroxidase-conjugated anti-mouse immunoglobulins [diluted 1:1,000; Agilent Technologies, Inc. (Agilent), Santa Clara, CA, USA, for H_2Mab-139-mG_{2a}-f], or with peroxidase-conjugated anti-rat immunoglobulins (diluted 1:1,000; Agilent, for RcMab-1). Finally, the protein bands were detected with a chemiluminescence reagent, ImmunoStar LD (Wako) using a Sayaca-Imager (DRC Co. Ltd., Tokyo, Japan).

2.7. IHC Analysis

A paraffin-embedded breast cancer tissue microarray (T8235721-5, BioChain Institute Inc., Eureka Drive Newark, CA, USA) was autoclaved in Envision FLEX TARGET RETRIEVAL SOLUTION High pH for 20 min. SuperBlock T20 (Thermo) was used for blocking. The sections were incubated with 10 µg/mL of H_2Mab-139-mG_{2a}-f for 1 h at room temperature and then treated with the EnVision+ Kit for mouse (Agilent) for 30 min. The chromogenic reaction was performed using 3,3′-diaminobenzidine tetrahydrochloride (DAB; Agilent). Hematoxylin (Wako) was used for the counterstaining. Leica DMD108 (Leica Microsystems GmbH, Wetzlar, Germany) was used to examine the sections and obtain images.

2.8. ADCC

Spleens were aseptically removed from six female BALB/c nude mice (five-week-old, Charles River Laboratories, Inc., Tokyo, Japan). Single-cell suspensions were obtained using a cell strainer (352360, BD). Erythrocytes were removed with the treatment of ice-cold distilled water. The splenocytes were used as effector cells.

H_2Mab-139-mG_{2a}-f-mediated ADCC was assayed as follows. Target cells (CHO-K1, CHO/HER2, BT-474, and MDA-MB-468) were labeled with 10 µg/ml Calcein AM (Thermo). The target cells (2×10^4 cells) were plated in 96-well plates and mixed with effector cells (effector/target cells ratio, 50), 100 µg/ml of H_2Mab-139-mG_{2a}-f or control mouse IgG_{2a} (mIgG_{2a}, Sigma-Aldrich, St. Louis, MO). Following incubation for 4.5 h at 37°C, the Calcein release into the medium was analyzed using a microplate reader (Power Scan HT; BioTek Instruments, Inc.,) with an excitation wavelength (485 nm) and an emission wavelength (538 nm).

Cytotoxicity (% lysis) was calculated as follows: % lysis = (E - S)/(M - S) x 100, where "E" is the fluorescence in cultures of both effector and target cells, "S" is the spontaneous fluorescence of only target cells, and "M" is the maximum fluorescence following the treatment with a lysis buffer [10 mM Tris-HCl (pH 7.4), 10 mM EDTA, and 0.5% Triton X-100].

2.9. CDC

The Calcein AM-labeled target cells (CHO-K1, CHO/HER2, BT-474, and MDA-MB-468) were plated in 96-well plates and mixed with rabbit complement (final dilution 1:10, Low-Tox-M Rabbit Complement; Cedarlane Laboratories, Hornby, ON, Canada) and 100 µg/ml of control mIgG_{2a} or

H2Mab-139-mG2a-f. Following incubation for 4.5 h at 37°C, Calcein release into the medium was measured.

2.10. Antitumor Activity of H2Mab-139-mG2a-f in Xenografts of CHO-K1, CHO/HER2, BT-474, and MDA-MB-468 Cells

CHO/HER2 (5×10^6 cells) resuspended in DMEM and mixed with BD Matrigel Matrix Growth Factor Reduced (BD) were subcutaneously injected into the left flank of BALB/c nude mice (female, 5 weeks old, Charles River Laboratories, Inc). On day 8 post-inoculation, 100 μg of H2Mab-139-mG2a-f (n=8) or control mouse IgG (mIgG, Wako) (n=8) in 100 μl PBS were intraperitoneally injected. On days 14 and 22, additional antibody injections were performed. The tumor volume was measured on days 8, 12, 14, 19, 22, and 26 after the inoculation of cells.

BT-474 and MDA-MB-468 (5×10^6 cells) were resuspended in DMEM and mixed with BD Matrigel Matrix Growth Factor Reduced (BD). They were subcutaneously injected into the left flank of BALB/c nude mice. On day 7 post-inoculation, 100 μg of H2Mab-139-mG2a-f (n=8) or control mIgG (n=8) in 100 μl PBS was intraperitoneally injected. On days 14 and 21, additional antibody injections were performed. The tumor volume was measured on days 7, 10, 14, 16, 21, 24, and 28 after the inoculation of cells.

Tumor volumes were determined as previously described [33,53–58].

2.11. Statistical Analyses

All data are presented as mean ± standard error of the mean (SEM). Welch's *t*-test was used for the statistical analyses in ADCC, CDC, and tumor weight. ANOVA with Sidak's post hoc test was used for the statistical analyses of tumor volume and mouse weight. GraphPad Prism 8 (GraphPad Software, Inc.) was utilized for the calculations. $P<0.05$ was considered to indicate a statistically significant difference.

3. Results

3.1. Detection of HER2 Using H2Mab-139-mG2a-f by Flow Cytometry

We previously established an anti-HER2 mAb (H2Mab-139, IgG1, kappa) by the immunization of HER2 ectodomain produced by glioblastoma LN229 cells [25]. H2Mab-139 was shown to be useful for flow cytometry, western blotting, and IHC [25]. In this study, we engineered a class-switched and defucosylated H2Mab-139 (H2Mab-139-mG2a-f) by fusing the V_H and V_L chains of H2Mab-139 with the C_H and C_L chains of mouse IgG2a, respectively (Figure 1A). We confirmed that H2Mab-139-mG2a-f was selectively recognized by anti-IgG2a, but not anti-IgG1 secondary antibodies in flow cytometry (Figure 1B). H2Mab-139-mG2a-f detected CHO/HER2 cells, but not parental CHO-K1 cells (Figure 1C). Furthermore, H2Mab-139-mG2a-f reacted HER2-positive breast cancer cell line, BT-474, but not the triple-negative breast cancer (TNBC) cell line, MDA-MB-468 (Figure 1D).

A kinetic analysis of the interactions of H2Mab-139-mG2a-f with CHO/HER2 and BT-474 was performed by flow cytometry. As shown in Figure. 1E, the K_D for the interaction of H2Mab-139-mG2a-f with CHO/HER2 and BT-474 were 3.9×10^{-9} M and 7.7×10^{-9} M, respectively. These results suggest that H2Mab-139-mG2a-f demonstrates a high affinity for HER2-expressing cells.

Preprints (www.preprints.org) | NOT PEER-REVIEWED | Posted: 4 July 2023 doi:10.20944/preprints202307.0169.v1

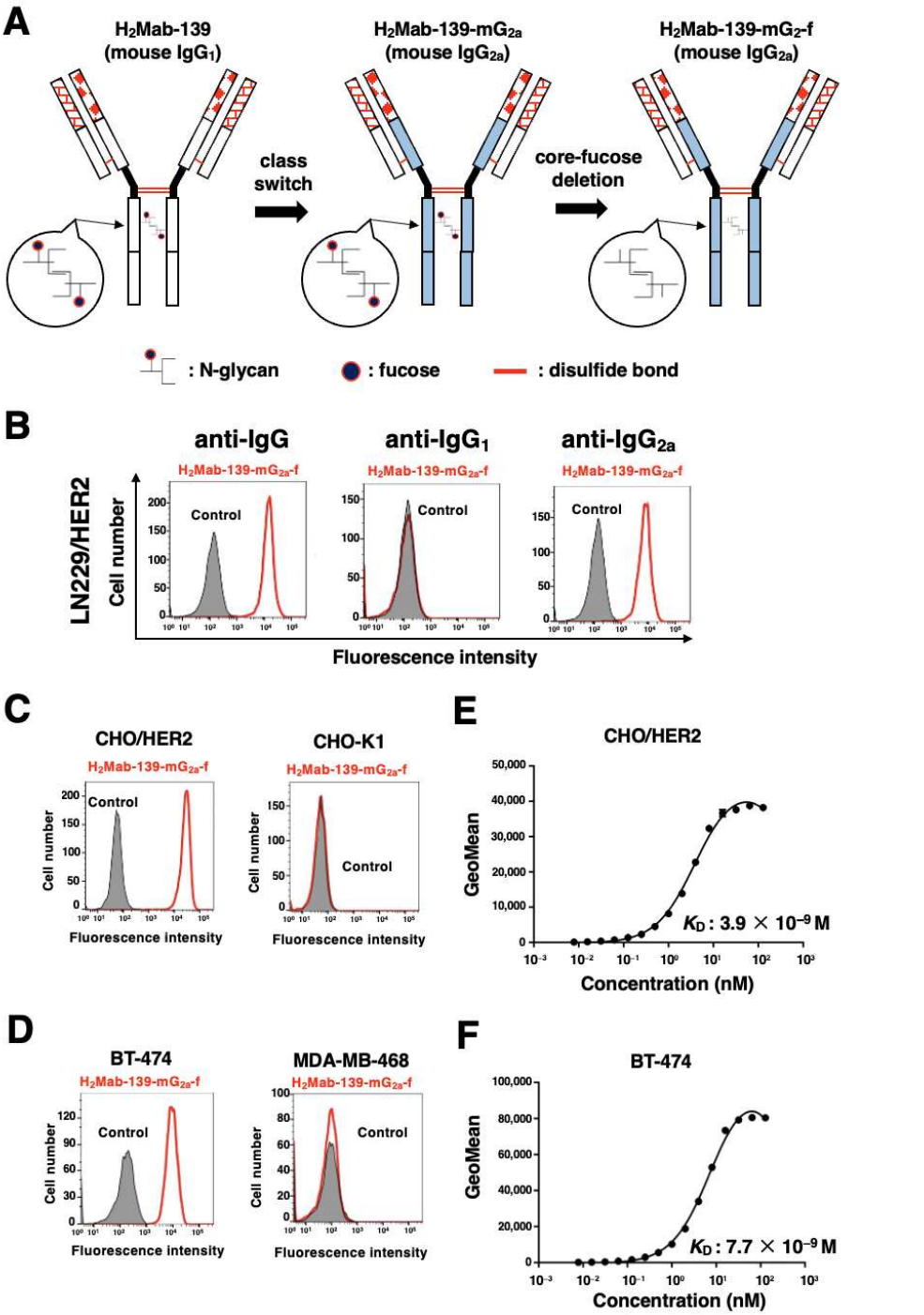

Figure 1. Flow cytometry using H2Mab-139-mG2a-f. (**A**) A core-fucose-deficient mouse IgG2a mAb, H2Mab-139-mG2a-f was produced from H2Mab-139 (mouse IgG1). (**B**) LN229/HER2 cells were treated with 1 μg/ml of H2Mab-139-mG2a-f or buffer control, followed by Alexa Fluor 488-conjugated anti-mouse IgG or Fluorescein-conjugated anti-mouse heavy chains (IgG1 and IgG2a). (**C**) CHO-K1 and CHO/HER2 cells were treated with 1 μg/ml of H2Mab-139-mG2a-f or buffer control, followed by Alexa Fluor 488-conjugated anti-mouse IgG. (**D**) BT-474 and MDA-MB-468 cells were treated with 1 μg/ml of H2Mab-139-mG2a-f or buffer control, followed by Alexa Fluor 488-conjugated anti-mouse IgG. (E,F) Determination of the binding affinity of H2Mab-139-mG2a-f using flow cytometry. CHO/HER2 (**E**) and BT-474 (**F**) cells were suspended in H2Mab-139-mG2a-f at indicated concentrations, followed by the addition of Alexa Fluor 488-conjugated anti-mouse IgG. Fluorescence data were analyzed using the SA3800 Cell Analyzer. The dissociation constant (*K*D) was calculated by GraphPad Prism 8.

Preprints (www.preprints.org) | NOT PEER-REVIEWED | Posted: 4 July 2023 doi:10.20944/preprints202307.0169.v1

3.2. Detection of HER2 Using H2Mab-139-mG2a-f in Western Blot and IHC Analyses

We next performed western blot analysis using H2Mab-139-mG2a-f. As shown in Figure 2A, H2Mab-139-mG2a-f strongly detected HER2 as more than 180-kDa bands in LN229/HER2 and BT-474 cells. H2Mab-139-mG2a-f faintly detected endogenous HER2 in LN229 cells, but not MDA-MB-468 cells. These results indicated that H2Mab-139-mG2a-f could detect exogenous and endogenous HER2 in western blot analysis.

Next, IHC analyses against the formalin-fixed paraffin-embedded (FFPE) sections of breast cancer tissue were performed using H2Mab-139-mG2a-f. As shown in Figure 2C–H, H2Mab-139-mG2a-f could distinguish HER2-strong positive (Figure 2C,D), moderate (Figure 2E,F), and negative (Figure 2G,H) breast cancers. The HER2-positive staining was mainly observed on the plasma membrane. We summarized the results of HER2 expression in breast cancer tissue array in supplementary Table S1. H2Mab-139-mG2a-f stained 10 out of 63 cases (16 %) of breast cancers. These results indicated that H2Mab-139-mG2a-f is also available for IHC analysis of FFPE tumor sections.

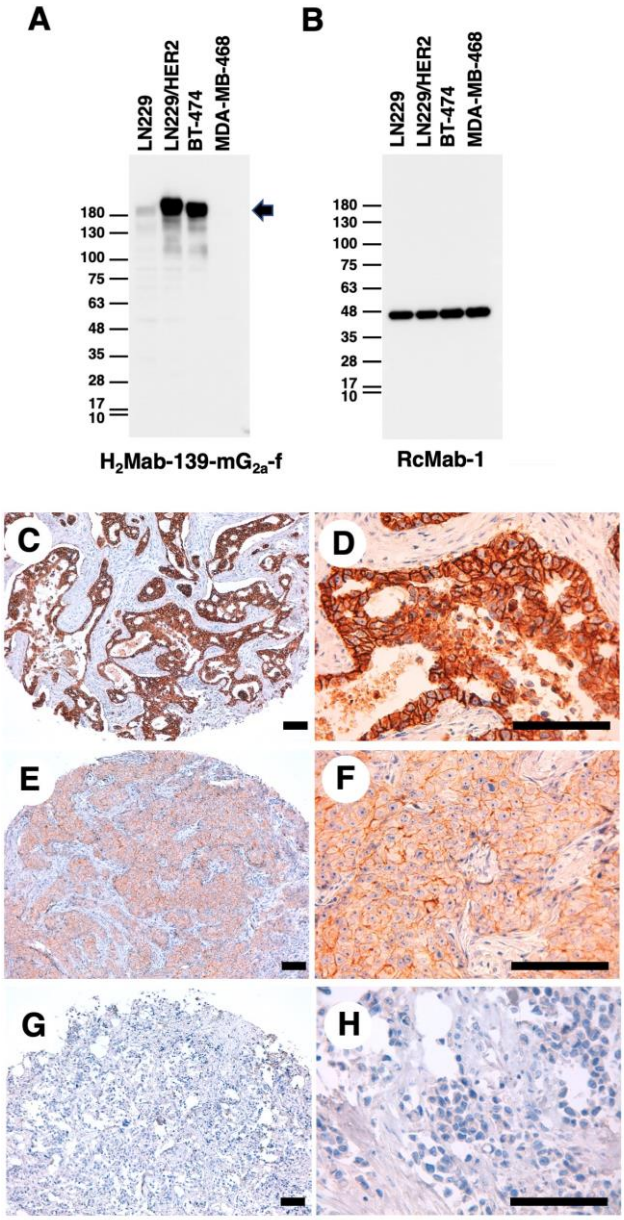

Figure 2. Western bot and IHC analyses using H2Mab-139-mG2a-f. (**A**,**B**) Western blotting using H2Mab-139-mG2a-f. The cell lysates of LN229, LN229/HER2, BT-474, and MDA-MB-468 were

Preprints (www.preprints.org) | NOT PEER-REVIEWED | Posted: 4 July 2023 doi:10.20944/preprints202307.0169.v1

electrophoresed and transferred onto polyvinylidene fluoride membranes. The membranes were incubated with 1 μg/mL of H2Mab-139-mG2a-f (**A**) or 1 μg/mL of RcMab-1 (an anti-IDH mAb) (**B**). The membranes were subsequently incubated with peroxidase-conjugated anti-rat immunoglobulins. The arrow indicates the predicted size of HER2 (~180 kDa). (**C**–**H**) After antigen retrieval, a breast cancer tissue array was incubated with 10 μg/mL of H2Mab-139-mG2a-f, followed by treatment with the Envision+ kit. The chromogenic reaction was conducted using 3,3′-diaminobenzidine tetrahydrochloride (DAB). The counterstaining was performed using hematoxylin. Scale bar = 100 μm.

3.3. ADCC and CDC by H2Mab-139-mG2a-f against CHO/HER2 Cells

We next investigated whether H2Mab-139-mG2a-f could exert ADCC against CHO/HER2 cells. H2Mab-139-mG2a-f showed ADCC (54.1% cytotoxicity) against CHO/HER2 cells more effectively than the control mouse IgG2a (18.8% cytotoxicity; P<0.05) (Figure 3A). There was no difference between H2Mab-139-mG2a-f and control mIgG2a about ADCC against CHO-K1 (Figure 3B).

We then examined whether H2Mab-139-mG2a-f could exhibit CDC against CHO/HER2 cells. As shown in Figure 3C, H2Mab-139-mG2a-f elicited a higher degree of CDC (62.5% cytotoxicity) in CHO/HER2 cells compared with that elicited by control mIgG2a (15.6% cytotoxicity; P<0.05). There was no difference between H2Mab-139-mG2a-f and control mIgG2a in CDC against CHO-K1 (Figure 3D). These results demonstrated that H2Mab-139-mG2a-f exerted higher levels of ADCC and CDC against CHO/HER2 cells.

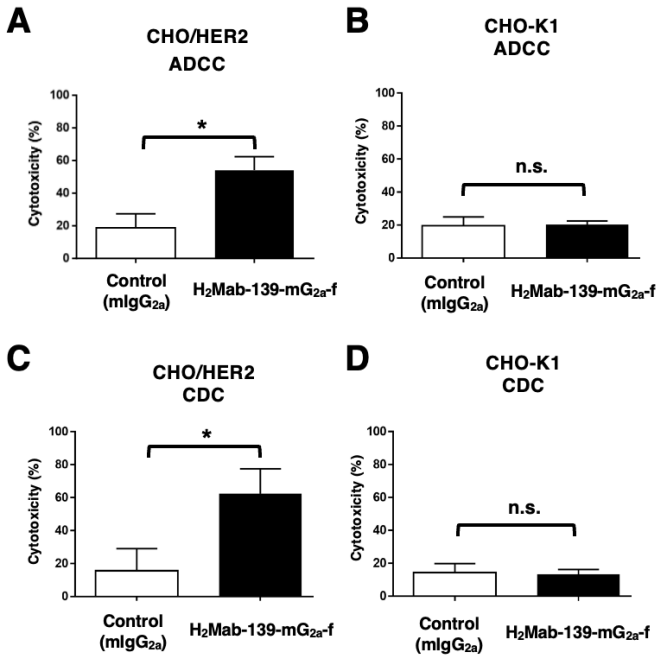

Figure 3. H2Mab-139-mG2a-f-mediated ADCC and CDC activities in CHO/HER2 and CHO-K1 cells. (**A**,**C**) ADCC induced by H2Mab-139-mG2a-f or control mouse IgG2a (mIgG2a) against CHO/HER2 (**A**) and CHO-K1 (**C**) cells. (**B**,**D**) CDC induced by H2Mab-139-mG2a-f or control mIgG2a against CHO/HER2 (**B**) and CHO-K1 (**D**) cells. Values are shown as mean ± SEM. Asterisks indicate statistical significance (*P< 0.05; Welch's *t*-test). n.s., not significant. ADCC, antibody-dependent cellular cytotoxicity; CDC, complement-dependent cytotoxicity.

3.4. Antitumor Effects of H2Mab-139-mG2a-f in the Mouse Xenografts of CHO/HER2 Cells

Following the inoculation of CHO/HER2, H2Mab-139-mG2a-f and control mIgG were intraperitoneally injected into CHO/HER2 xenograft tumor-bearing mice on days 8, 14, and 22. On days 8, 12, 14, 19, 22, and 26 after the injection, the tumor volume was measured. The H2Mab-139-mG2a-f administration resulted in a significant reduction of tumors on days 19 (P<0.01), 22 (P<0.01), and 26 (P<0.01) compared with that of mIgG (Figure 4A). The H2Mab-139-mG2a-f administration

Preprints (www.preprints.org) | NOT PEER-REVIEWED | Posted: 4 July 2023 doi:10.20944/preprints202307.0169.v1

resulted in a 52% reduction of the volume compared with that of the control mIgG on day 26 post-injection.

The weight of CHO/HER2 tumors treated with H2Mab-139-mG2a-f was significantly lower than that treated with mIgG (66% reduction; P<0.05; Figure 4B). CHO/HER2 tumors that were resected from mice on day 26 are demonstrated in Figure 4C.

The body weight loss and skin disorder were not observed in CHO/HER2 tumor-bearing mice (Figure 4D). The mice on day 26 were shown in supplementary Figure S1.

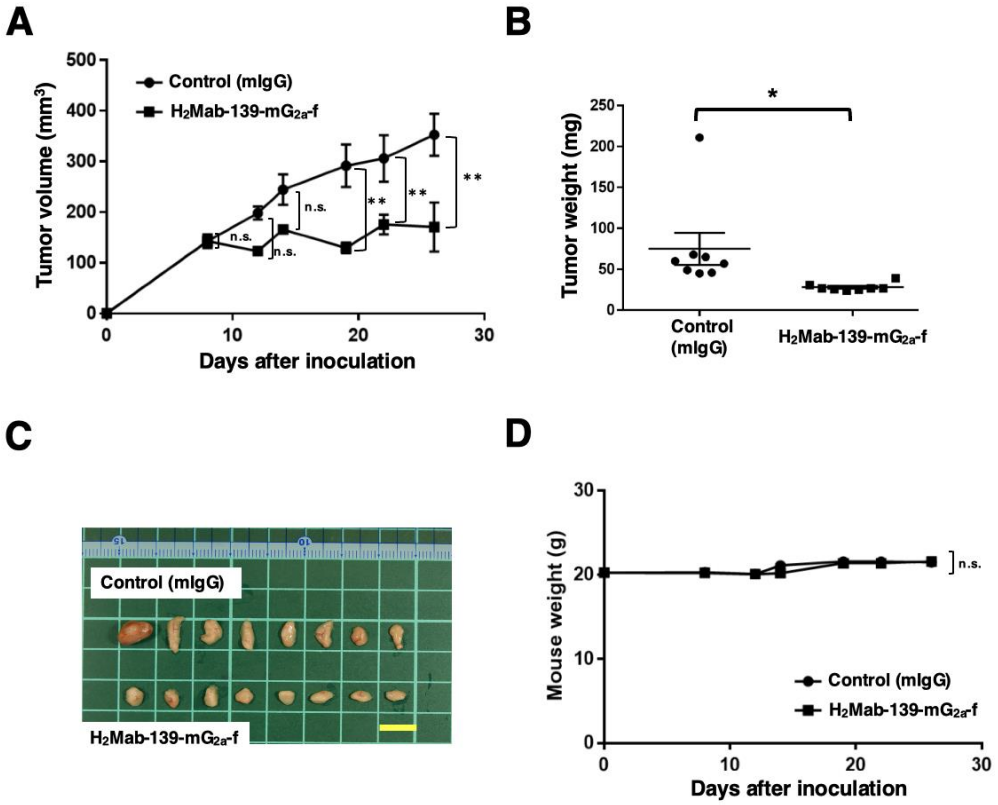

Figure 4. Antitumor activity of H2Mab-139-mG2a-f against CHO/HER2 xenograft. (**A**) CHO/HER2 cells (5 × 10^6 cells) were subcutaneously injected into BALB/c nude mice. On day 8, 100 μg of H2Mab-139-mG2a-f or control normal mouse IgG (mIgG) was injected intraperitoneally into mice. Additional antibodies were injected on days 14 and 22. The tumor volume was measured on days 8, 12, 14, 19, 22, and 26 after the injection. Values are presented as the mean ± SEM. **P<0.01 (ANOVA and Sidak's multiple comparisons test). (**B**) Tumor weight (day 28) was measured from excised CHO/HER2 xenograft tumors. Values are presented as the mean ± SEM. * P<0.05 (Welch's *t*-test). (**C**) The appearance of CHO/HER2 xenograft tumors from the control mIgG and H2Mab-139-mG2a-f treated mice on day 28 (scale bar, 1 cm). (**D**) Mice weight in mIgG and H2Mab-139-mG2a-f treated groups. n.s., not significant.

3.5. ADCC and CDC by H2Mab-139-mG2a-f against BT-474 and MDA-MB-468 Cells

It was investigated whether H2Mab-139-mG2a-f was capable of mediating ADCC against BT-474 and MDA-MB-468 cells. As revealed in Figure 5A, H2Mab-139-mG2a-f showed ADCC (37.6% cytotoxicity) against BT-474 cells more potently than did the control mIgG2a (3.8% cytotoxicity; P<0.01). It was next investigated whether H2Mab-139-mG2a-f exhibited CDC against BT-474 cells. H2Mab-139-mG2a-f induced a higher degree of CDC (70.6% cytotoxicity) in BT-474 cells s compared with that induced by control mIgG2a (34.6% cytotoxicity; P<0.01) (Figure 5B). However, there was no difference between H2Mab-139-mG2a-f and control mIgG2a in ADCC (Figure 5C) and CDC (Figure

Preprints (www.preprints.org) | NOT PEER-REVIEWED | Posted: 4 July 2023 doi:10.20944/preprints202307.0169.v1

5D) against MDA-MB-468. These results demonstrated that H2Mab-139-mG2a-f exhibited higher levels of ADCC and CDC against HER2-positive BT-474 cells.

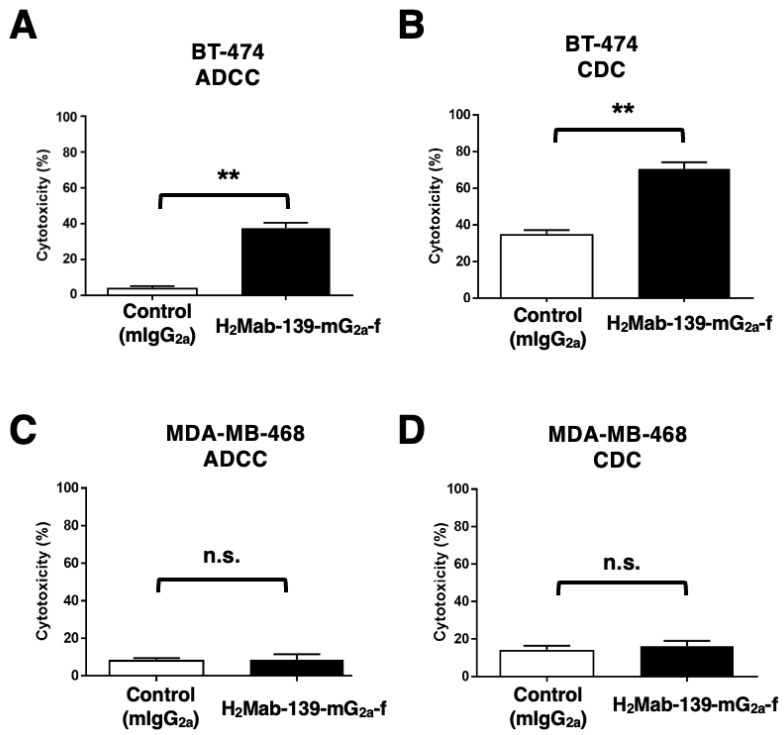

Figure 5. H2Mab-139-mG2a-f-mediated ADCC and CDC activities in BT-474 (HER2-positive) and MDA-MB-468 (TNBC) cells. (**A**,**C**) ADCC induced by H2Mab-139-mG2a-f or control mIgG2a against BT-474 (**A**) and MDA-MB-468 (**C**) cells. (**B**,**D**) CDC induced by H2Mab-139-mG2a-f or control mIgG2a against BT-474 (**B**) and MDA-MB-468 (**D**) cells. Values are shown as mean ± SEM. Asterisks indicate statistical significance (**P < 0.01; Welch's *t*-test). n.s., not significant. ADCC, antibody-dependent cellular cytotoxicity; CDC, complement-dependent cytotoxicity.

3.6. Antitumor Effects of H2Mab-139-mG2a-f in BT-474 and MDA-MB-468 Xenografts

In the BT-474 xenograft models, H2Mab-139-mG2a-f and control mIgG were injected intraperitoneally on days 7, 14, and 21 following BT-474 inoculation. The tumor volume was measured on days 7, 10, 14, 16, 21, 24, and 28 after the inoculation. The H2Mab-139-mG2a-f administration resulted in a significant reduction in BT-474 xenograft on days 21 (P<0.01), 24 (P<0.01), and 28 (P<0.01) compared with that of the control mIgG (Figure 6A). The H2Mab-139-mG2a-f administration resulted in a 36% reduction of tumor volume compared with that of the control mIgG on day 28.

Tumors from the H2Mab-139-mG2a-f-treated mice weighed significantly less than those from the control mIgG -treated mice (45% reduction; P<0.01, Figure 6C). Tumors that were resected from mice on day 28 are demonstrated in Figure 6E.

In the MDA-MB-468 xenograft models, H2Mab-139-mG2a-f and control mIgG were injected intraperitoneally into mice on days 7, 14, and 21 after the inoculation of MDA-MB-468 cells. The tumor volume was measured on days 7, 10, 14, 16, 21, 24, and 28. No difference was observed between H2Mab-139-mG2a-f and control mIgG about MDA-MB-468 xenograft volume (Figure 6B) and weight (Figure 6D). MDA-MB-468 tumors that were resected from mice on day 28 are demonstrated in Figure 6F.

The body weight loss was not observed in both BT-474 and MDA-MB-468 xenograft -bearing mice (Figure 6G,H). The mice on day 28 about BT-474 and MDA-MB-468 xenograft were demonstrated in supplementary Figure S2.

Preprints (www.preprints.org) | NOT PEER-REVIEWED | Posted: 4 July 2023 doi:10.20944/preprints202307.0169.v1

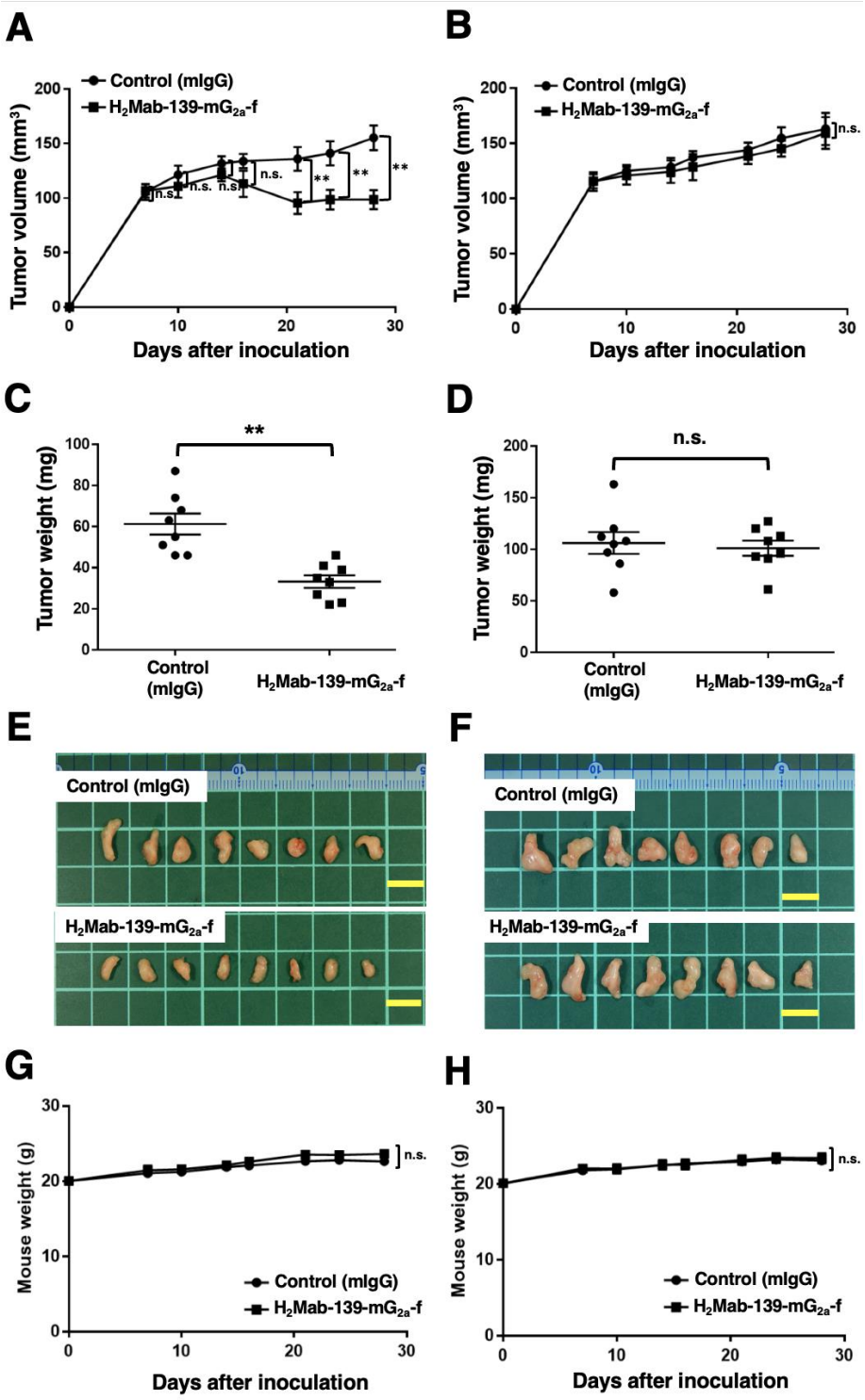

Figure 6. Antitumor activity of H2Mab-139-mG2a-f against BT-474 and MDA-MB-468 xenografts. (**A, B**) BT-474 (**A**) and MDA-MB-468 (**B**) cells (5×10^6 cells) were subcutaneously injected into BALB/c nude mice. On day 7, 100 μg of H2Mab-139-mG2a-f or control normal mouse IgG (mIgG) were injected intraperitoneally into mice. Additional antibodies were injected on days 14 and 21. The tumor volume was measured on days 7, 10, 14, 16, 21, 24, and 28 after the inoculation. Values are presented as the mean ± SEM. **P <0.01 (ANOVA and Sidak's multiple comparisons test). (**C,D**) Tumor weight (day 28) was measured from excised BT-474 (**C**) and MDA-MB-468 (**D**) xenograft tumors. Values are presented as the mean ± SEM. **P <0.01 (Welch's *t*-test). (**E, F**) The appearance of BT-474 (**E**) and MDA-MB-468 (**F**) xenograft tumors from the control mIgG and H2Mab-139-mG2a-f-treated mice on day 28 (scale bar, 1 cm). (**G,H**) The body weight of BT-474 (G) and MDA-MB-468 (H) xenograft-bearing mice treated with mIgG and H2Mab-139-mG2a-f. n.s., not significant.

 doi:10.20944/preprints202307.0169.v1

4. Discussion

For the clinical treatment of metastatic breast cancer, trastuzumab is administered for patients with HER2-overexpressing tumors, which are defined by strong and complete IHC membranous staining of more than 10% of cells (IHC 3+) and/or *in situ* hybridization (ISH)-amplified. Based on clinical studies, the 5th the European School of Oncology and the European Society of Medical Oncology guidelines for advanced breast cancer (ABC 5) and the National Comprehensive Cancer Network guidelines consider trastuzumab (anti-HER2 domain IV mAb), pertuzumab (anti-HER2 domain II mAb), and docetaxel as the standard of care for first-line treatment of HER2-positive metastatic breast cancer [59]. However, most deaths in the study were due to breast cancer [21]. Therefore, better treatments including novel combination therapies and novel modalities are still needed. In this study, we evaluated a novel anti-HER2 domain I mAb, H_2Mab-139-mG_{2a}-f, and showed the ADCC activity *in vitro* (Figures 3 and 5) and antitumor effect *in vivo* (Figures 4 and 6). Therefore, H_2Mab-139-mG_{2a}-f could be an antibody treatment regimen for HER2-positive breast cancer.

Cryo-electron microscopy (cryo-EM) is now recognized as the primary technique for determining the structure of protein complexes. The cryo-EM structure of HER2-trastuzumab-pertuzumab revealed that trastuzumab and pertuzumab simultaneously bind to HER2 with little conformational change [60]. Due to the success of the combination therapy of trastuzumab and pertuzumab in clinic [59], various bispecific Abs containing variable regions of trastuzumab and pertuzumab were evaluated. However, the cryo-EM structure of HER2-trastuzumab-pertuzumab suggested that the two Fab arms of one bispecific Ab cannot bind to both domains II and IV of one HER2 [60]. We previously produced a bispecific Ab against EGFR and HER2 from our established anti-EGFR mAb (EMab-134) and an anti-HER2 mAb (H_2Mab-77) [61]. The bispecific Ab possesses the tetravalent structure by fusing the single chain Fv of H_2Mab-77 at the light chains of EMab-134 and showed the antitumor effect in mouse xenograft model [61]. Since we can produce the different types of bispecific Abs and have various clones of anti-HER2 mAbs including H_2Mab-139 (see Supplementary Materials), we will investigate the activity in the future study.

The structures of the HER2–HER3–NRG1β complex, revealed by cryo-EM, exhibit a dynamic dimer interface. In the complex, the NRG1β-bound HER3 dimerization arm remains unresolved due to the lack of a ligand-induced conformational change in the apo HER2 monomer, which is essential for the formation of the HER3 dimerization arm-binding pocket [22]. In contrast, the most frequent oncogenic HER2 mutation (S310F/Y) was found primarily in cancers without HER2 overexpression. The HER2 S310 is localized in the dimerization arm-binding pocket of domain II [62]. The structures of HER2 (S310F)–HER3–NRG1β complex exhibited stabilizing interactions with the HER3 dimerization arm and compensate for the inability of HER2 to undergo a needed conformational change [22]. Furthermore, HER2–HER3 and HER2 (S310F)–HER3 retain the ability to bind to trastuzumab, but the mutant complex does not bind to pertuzumab [22]. These results suggest that pertuzumab is less effective at targeting cancers driven by HER2 (S310F), and different epitope-possessing anti-HER2 mAbs including H_2Mab-139 could be required for the combination therapy with trastuzumab.

Trastuzumab-based antibody-drug conjugates (ADCs) such as trastuzumab-deruxtecan (T-DXd) have been evaluated. These ADCs rely on the direct cytotoxicity of the released DXd (a DNA topoisomerase I inhibitor) following endocytosis of the HER2-bound mAbs-drug conjugate [63]. T-DXd initially exhibited beneficial outcomes in patients with metastatic breast cancer, who had undergone multiple anti-HER2-targeting treatments [64]. Currently, various clinical trials are evaluating the efficacy of T-DXd. Based on studies, T-DXd has been approved in not only HER2-positive breast cancer [65–67], but also HER2-mutant lung cancer [68] and HER2-low (IHC 1+ or IHC 2+ / ISH-non-amplified) advanced breast cancer [69].

Given that approximately half of all breast cancers are classifiable as HER2-low [70], a greater number of patients may benefit from T-DXd therapy. These results have had a significant on the field of breast oncology, particularly in the future clinical diagnostics of HER2-low breast cancer. As a result, future treatment algorithms for both hormone receptor-positive and TNBC are anticipated to

change [71]. There are several challenges in elucidating the biological roles and pathological significance of HER2-low [72]. Since our H2Mab-139 is applicable for IHC (Figure 2), it would be valuable to compare its reactivity with approved anti-HER2 diagnostic mAbs such as HercepTest™ and PATHWAY®.

We achieved increased ADCC activity of H2Mab-139-mG2a-f through class switching and a core fucose deficiency on the *N*-glycan in the Fc region, which promotes the binding of Fc to FcγRIIIa on effector cells [73]. This technique is also applied to mogamulizumab (Poteligeo), a defucosylated humanized mAb targeting CCR4 [74]. In contrast, margetuximab is derived from trastuzumab and shares the same epitope with HER2. Five amino acid substitutions in the Fc domain of margetuximab (human IgG1) achieve increased binding to FcγRIIIa and reduced binding to an inhibitory FcγR, FcγRIIb, when compared to trastuzumab [9]. We are going to apply the strategy to potentiate the ADCC activity when we generate the humanized H2Mab-139 mAb.

Previously, we established H2Mab-139 using cancer cell-produced HER2 ectodomain as an immunogen. This methodology is essential for the development of cancer-specific mAbs (CasMabs). We have developed CasMabs that target podoplanin (PDPN) [75–77] and podocalyxin [78], which recognize the aberrant glycosylation patterns typical of cancer cells [79]. Anti-PDPN-CasMabs are currently applied to CAR-T therapy in preclinical models [44,80,81]. For the development of anti-HER2 CasMab, we need to perform further screening of our already established anti-HER2 mAbs (more than 200 clones), comparing their reactivity against normal cells. Anti-HER2 CasMabs could be employed in designing modalities including ADCs and CAR-T.

Supplementary Materials: We listed the information of anti-HER2 mAbs in our original "Antibody Bank" [http://www.med-tohoku-antibody.com/topics/001_paper_antibody_PDIS.htm#HER2 (accessed on 4 July 2023)]. Supplementary Figure S1, Body appearance in CHO/HER2 xenografts-implanted mice treated with mIgG and H2Mab-139-mG2a-f on day 26. Supplementary Figure S2, Body appearance in (**A**) BT-474 and (**B**) MDA-MB-468 xenografts-implanted mice treated with mIgG and H2Mab-139-mG2a-f on day 28. Supplementary Table S1, IHC analysis using H2Mab-139-mG2a-f against breast cancer tissue array.

Author Contributions: H.S., T.O. and R.N. performed the experiments. M.K.K. and Y.K. designed the experiments. H.S., R.N. and Y.K. analyzed the data. H.S. and Y.K. wrote the manuscript. All authors have read and agreed to the manuscript.

Funding: This research was supported in part by Japan Agency for Medical Research and Development (AMED) under Grant Numbers: JP23ama121008 (to Y.K.), JP23am0401013 (to Y.K.), and JP23ck0106730 (to Y.K.), and by the Japan Society for the Promotion of Science (JSPS) Grants-in-Aid for Scientific Research (KAKENHI) grant nos. 22K06995 (to H.S.), 21K07168 (to M.K.K.), and 22K07224 (to Y.K.).

Institutional Review Board Statement: Animal experiments were approved by the Institutional Committee for Experiments of the Institute of Microbial Chemistry (approval no. 2022-056, 2023-001, and 2023-018).

Informed Consent Statement: Not applicable.

Data Availability Statement: The data presented in this study are available in the article and supplementary material.

Acknowledgments: The authors would like to thank Shun-ichi Ohba and Akiko Harakawa (Institute of Microbial Chemistry [BIKAKEN], Numazu, the Microbial Chemistry Research Foundation) for technical assistance with animal experiments.

Conflicts of Interest: The authors have no conflict of interest to declare.

References

1. Yarden, Y.; Sliwkowski, M.X. Untangling the ErbB signalling network. *Nat Rev Mol Cell Biol* **2001**, *2*, 127-137, doi:10.1038/35052073.
2. Yarden, Y.; Pines, G. The ERBB network: at last, cancer therapy meets systems biology. *Nat Rev Cancer* **2012**, *12*, 553-563, doi:10.1038/nrc3309.
3. Stern, D.F.; Kamps, M.P. EGF-stimulated tyrosine phosphorylation of p185neu: a potential model for receptor interactions. *Embo j* **1988**, *7*, 995-1001, doi:10.1002/j.1460-2075.1988.tb02906.x.

4. Wallasch, C.; Weiss, F.U.; Niederfellner, G.; Jallal, B.; Issing, W.; Ullrich, A. Heregulin-dependent regulation of HER2/neu oncogenic signaling by heterodimerization with HER3. *Embo j* **1995**, *14*, 4267-4275, doi:10.1002/j.1460-2075.1995.tb00101.x.
5. Slamon, D.J.; Clark, G.M.; Wong, S.G.; Levin, W.J.; Ullrich, A.; McGuire, W.L. Human breast cancer: correlation of relapse and survival with amplification of the HER-2/neu oncogene. *Science* **1987**, *235*, 177-182, doi:10.1126/science.3798106.
6. Van Cutsem, E.; Bang, Y.J.; Feng-Yi, F.; Xu, J.M.; Lee, K.W.; Jiao, S.C.; Chong, J.L.; López-Sanchez, R.I.; Price, T.; Gladkov, O.; et al. HER2 screening data from ToGA: targeting HER2 in gastric and gastroesophageal junction cancer. *Gastric Cancer* **2015**, *18*, 476-484, doi:10.1007/s10120-014-0402-y.
7. Cho, H.S.; Mason, K.; Ramyar, K.X.; Stanley, A.M.; Gabelli, S.B.; Denney, D.W., Jr.; Leahy, D.J. Structure of the extracellular region of HER2 alone and in complex with the Herceptin Fab. *Nature* **2003**, *421*, 756-760, doi:10.1038/nature01392.
8. Tsao, L.C.; Force, J.; Hartman, Z.C. Mechanisms of Therapeutic Antitumor Monoclonal Antibodies. *Cancer Res* **2021**, *81*, 4641-4651, doi:10.1158/0008-5472.Can-21-1109.
9. Essadi, I.; Benbrahim, Z.; Kaakoua, M.; Reverdy, T.; Corbaux, P.; Freyer, G. HER2-Positive Metastatic Breast Cancer: Available Treatments and Current Developments. *Cancers (Basel)* **2023**, *15*, doi:10.3390/cancers15061738.
10. Slamon, D.J.; Leyland-Jones, B.; Shak, S.; Fuchs, H.; Paton, V.; Bajamonde, A.; Fleming, T.; Eiermann, W.; Wolter, J.; Pegram, M.; et al. Use of chemotherapy plus a monoclonal antibody against HER2 for metastatic breast cancer that overexpresses HER2. *N Engl J Med* **2001**, *344*, 783-792, doi:10.1056/nejm200103153441101.
11. Bang, Y.J.; Van Cutsem, E.; Feyereislova, A.; Chung, H.C.; Shen, L.; Sawaki, A.; Lordick, F.; Ohtsu, A.; Omuro, Y.; Satoh, T.; et al. Trastuzumab in combination with chemotherapy versus chemotherapy alone for treatment of HER2-positive advanced gastric or gastro-oesophageal junction cancer (ToGA): a phase 3, open-label, randomised controlled trial. *Lancet* **2010**, *376*, 687-697, doi:10.1016/s0140-6736(10)61121-x.
12. Maadi, H.; Soheilifar, M.H.; Choi, W.S.; Moshtaghian, A.; Wang, Z. Trastuzumab Mechanism of Action; 20 Years of Research to Unravel a Dilemma. *Cancers (Basel)* **2021**, *13*, doi:10.3390/cancers13143540.
13. Musolino, A.; Gradishar, W.J.; Rugo, H.S.; Nordstrom, J.L.; Rock, E.P.; Arnaldez, F.; Pegram, M.D. Role of Fcγ receptors in HER2-targeted breast cancer therapy. *J Immunother Cancer* **2022**, *10*, doi:10.1136/jitc-2021-003171.
14. Nordstrom, J.L.; Gorlatov, S.; Zhang, W.; Yang, Y.; Huang, L.; Burke, S.; Li, H.; Ciccarone, V.; Zhang, T.; Stavenhagen, J.; et al. Anti-tumor activity and toxicokinetics analysis of MGAH22, an anti-HER2 monoclonal antibody with enhanced Fcγ receptor binding properties. *Breast Cancer Res* **2011**, *13*, R123, doi:10.1186/bcr3069.
15. McAndrew, N.P. Updates on targeting human epidermal growth factor receptor 2-positive breast cancer: what's to know in 2021. *Curr Opin Obstet Gynecol* **2022**, *34*, 41-45, doi:10.1097/gco.0000000000000762.
16. Rugo, H.S.; Im, S.A.; Cardoso, F.; Cortés, J.; Curigliano, G.; Musolino, A.; Pegram, M.D.; Wright, G.S.; Saura, C.; Escrivá-de-Romaní, S.; et al. Efficacy of Margetuximab vs Trastuzumab in Patients With Pretreated ERBB2-Positive Advanced Breast Cancer: A Phase 3 Randomized Clinical Trial. *JAMA Oncol* **2021**, *7*, 573-584, doi:10.1001/jamaoncol.2020.7932.
17. Golay, J.; Taylor, R.P. The Role of Complement in the Mechanism of Action of Therapeutic Anti-Cancer mAbs. *Antibodies (Basel)* **2020**, *9*, doi:10.3390/antib9040058.
18. Reis, E.S.; Mastellos, D.C.; Ricklin, D.; Mantovani, A.; Lambris, J.D. Complement in cancer: untangling an intricate relationship. *Nat Rev Immunol* **2018**, *18*, 5-18, doi:10.1038/nri.2017.97.
19. Franklin, M.C.; Carey, K.D.; Vajdos, F.F.; Leahy, D.J.; de Vos, A.M.; Sliwkowski, M.X. Insights into ErbB signaling from the structure of the ErbB2-pertuzumab complex. *Cancer Cell* **2004**, *5*, 317-328, doi:10.1016/s1535-6108(04)00083-2.
20. Badache, A.; Hynes, N.E. A new therapeutic antibody masks ErbB2 to its partners. *Cancer Cell* **2004**, *5*, 299-301, doi:10.1016/s1535-6108(04)00088-1.
21. Swain, S.M.; Baselga, J.; Kim, S.B.; Ro, J.; Semiglazov, V.; Campone, M.; Ciruelos, E.; Ferrero, J.M.; Schneeweiss, A.; Heeson, S.; et al. Pertuzumab, trastuzumab, and docetaxel in HER2-positive metastatic breast cancer. *N Engl J Med* **2015**, *372*, 724-734, doi:10.1056/NEJMoa1413513.
22. Diwanji, D.; Trenker, R.; Thaker, T.M.; Wang, F.; Agard, D.A.; Verba, K.A.; Jura, N. Structures of the HER2-HER3-NRG1β complex reveal a dynamic dimer interface. *Nature* **2021**, *600*, 339-343, doi:10.1038/s41586-021-04084-z.
23. Itai, S.; Fujii, Y.; Kaneko, M.K.; Yamada, S.; Nakamura, T.; Yanaka, M.; Saidoh, N.; Chang, Y.W.; Handa, S.; Takahashi, M.; et al. H2Mab-77 is a Sensitive and Specific Anti-HER2 Monoclonal Antibody Against Breast Cancer. *Monoclon Antib Immunodiagn Immunother* **2017**, *36*, 143-148, doi:10.1089/mab.2017.0026.

24. Yamada, S.; Itai, S.; Nakamura, T.; Chang, Y.W.; Harada, H.; Suzuki, H.; Kaneko, M.K.; Kato, Y. Establishment of H(2)Mab-119, an Anti-Human Epidermal Growth Factor Receptor 2 Monoclonal Antibody, Against Pancreatic Cancer. *Monoclon Antib Immunodiagn Immunother* **2017**, *36*, 287-290, doi:10.1089/mab.2017.0050.
25. Kaneko, M.K.; Yamada, S.; Itai, S.; Kato, Y. Development of an Anti-HER2 Monoclonal Antibody H2Mab-139 Against Colon Cancer. *Monoclon Antib Immunodiagn Immunother* **2018**, *37*, 59-62, doi:10.1089/mab.2017.0052.
26. Li, G.; Suzuki, H.; Ohishi, T.; Asano, T.; Tanaka, T.; Yanaka, M.; Nakamura, T.; Yoshikawa, T.; Kawada, M.; Kaneko, M.K.; et al. Antitumor activities of a defucosylated anti-EpCAM monoclonal antibody in colorectal carcinoma xenograft models. *Int J Mol Med* **2023**, *51*, doi:10.3892/ijmm.2023.5221.
27. Nanamiya, R.; Takei, J.; Ohishi, T.; Asano, T.; Tanaka, T.; Sano, M.; Nakamura, T.; Yanaka, M.; Handa, S.; Tateyama, N.; et al. Defucosylated Anti-Epidermal Growth Factor Receptor Monoclonal Antibody (134-mG(2a)-f) Exerts Antitumor Activities in Mouse Xenograft Models of Canine Osteosarcoma. *Monoclon Antib Immunodiagn Immunother* **2022**, *41*, 1-7, doi:10.1089/mab.2021.0036.
28. Kawabata, H.; Suzuki, H.; Ohishi, T.; Kawada, M.; Kaneko, M.K.; Kato, Y. A Defucosylated Mouse Anti-CD10 Monoclonal Antibody (31-mG(2a)-f) Exerts Antitumor Activity in a Mouse Xenograft Model of CD10-Overexpressed Tumors. *Monoclon Antib Immunodiagn Immunother* **2022**, *41*, 59-66, doi:10.1089/mab.2021.0048.
29. Kawabata, H.; Ohishi, T.; Suzuki, H.; Asano, T.; Kawada, M.; Suzuki, H.; Kaneko, M.K.; Kato, Y. A Defucosylated Mouse Anti-CD10 Monoclonal Antibody (31-mG(2a)-f) Exerts Antitumor Activity in a Mouse Xenograft Model of Renal Cell Cancers. *Monoclon Antib Immunodiagn Immunother* **2022**, doi:10.1089/mab.2021.0049.
30. Asano, T.; Tanaka, T.; Suzuki, H.; Li, G.; Ohishi, T.; Kawada, M.; Yoshikawa, T.; Kaneko, M.K.; Kato, Y. A Defucosylated Anti-EpCAM Monoclonal Antibody (EpMab-37-mG(2a)-f) Exerts Antitumor Activity in Xenograft Model. *Antibodies (Basel)* **2022**, *11*, doi:10.3390/antib11040074.
31. Tateyama, N.; Nanamiya, R.; Ohishi, T.; Takei, J.; Nakamura, T.; Yanaka, M.; Hosono, H.; Saito, M.; Asano, T.; Tanaka, T.; et al. Defucosylated Anti-Epidermal Growth Factor Receptor Monoclonal Antibody 134-mG(2a)-f Exerts Antitumor Activities in Mouse Xenograft Models of Dog Epidermal Growth Factor Receptor-Overexpressed Cells. *Monoclon Antib Immunodiagn Immunother* **2021**, *40*, 177-183, doi:10.1089/mab.2021.0022.
32. Takei, J.; Ohishi, T.; Kaneko, M.K.; Harada, H.; Kawada, M.; Kato, Y. A defucosylated anti-PD-L1 monoclonal antibody 13-mG(2a)-f exerts antitumor effects in mouse xenograft models of oral squamous cell carcinoma. *Biochem Biophys Rep* **2020**, *24*, 100801, doi:10.1016/j.bbrep.2020.100801.
33. Takei, J.; Kaneko, M.K.; Ohishi, T.; Hosono, H.; Nakamura, T.; Yanaka, M.; Sano, M.; Asano, T.; Sayama, Y.; Kawada, M.; et al. A defucosylated antiCD44 monoclonal antibody 5mG2af exerts antitumor effects in mouse xenograft models of oral squamous cell carcinoma. *Oncol Rep* **2020**, *44*, 1949-1960, doi:10.3892/or.2020.7735.
34. Yamane-Ohnuki, N.; Kinoshita, S.; Inoue-Urakubo, M.; Kusunoki, M.; Iida, S.; Nakano, R.; Wakitani, M.; Niwa, R.; Sakurada, M.; Uchida, K.; et al. Establishment of FUT8 knockout Chinese hamster ovary cells: an ideal host cell line for producing completely defucosylated antibodies with enhanced antibody-dependent cellular cytotoxicity. *Biotechnol Bioeng* **2004**, *87*, 614-622, doi:10.1002/bit.20151.
35. Kato, Y.; Kaneko, M.K.; Kuno, A.; Uchiyama, N.; Amano, K.; Chiba, Y.; Hasegawa, Y.; Hirabayashi, J.; Narimatsu, H.; Mishima, K.; et al. Inhibition of tumor cell-induced platelet aggregation using a novel anti-podoplanin antibody reacting with its platelet-aggregation-stimulating domain. *Biochem Biophys Res Commun* **2006**, *349*, 1301-1307, doi:10.1016/j.bbrc.2006.08.171.
36. Ishikawa, A.; Waseda, M.; Ishii, T.; Kaneko, M.K.; Kato, Y.; Kaneko, S. Improved anti-solid tumor response by humanized anti-podoplanin chimeric antigen receptor transduced human cytotoxic T cells in an animal model. *Genes Cells* **2022**, *27*, 549-558, doi:10.1111/gtc.12972.
37. Tamura-Sakaguchi, R.; Aruga, R.; Hirose, M.; Ekimoto, T.; Miyake, T.; Hizukuri, Y.; Oi, R.; Kaneko, M.K.; Kato, Y.; Akiyama, Y.; et al. Moving toward generalizable NZ-1 labeling for 3D structure determination with optimized epitope-tag insertion. *Acta Crystallogr D Struct Biol* **2021**, *77*, 645-662, doi:10.1107/S2059798321002527.
38. Kaneko, M.K.; Ohishi, T.; Nakamura, T.; Inoue, H.; Takei, J.; Sano, M.; Asano, T.; Sayama, Y.; Hosono, H.; Suzuki, H.; et al. Development of Core-Fucose-Deficient Humanized and Chimeric Anti-Human Podoplanin Antibodies. *Monoclon Antib Immunodiagn Immunother* **2020**, *39*, 167-174, doi:10.1089/mab.2020.0019.

39. Fujii, Y.; Matsunaga, Y.; Arimori, T.; Kitago, Y.; Ogasawara, S.; Kaneko, M.K.; Kato, Y.; Takagi, J. Tailored placement of a turn-forming PA tag into the structured domain of a protein to probe its conformational state. *J Cell Sci* **2016**, *129*, 1512-1522, doi:10.1242/jcs.176685.
40. Abe, S.; Kaneko, M.K.; Tsuchihashi, Y.; Izumi, T.; Ogasawara, S.; Okada, N.; Sato, C.; Tobiume, M.; Otsuka, K.; Miyamoto, L.; et al. Antitumor effect of novel anti-podoplanin antibody NZ-12 against malignant pleural mesothelioma in an orthotopic xenograft model. *Cancer Sci* **2016**, *107*, 1198-1205, doi:10.1111/cas.12985.
41. Kaneko, M.K.; Abe, S.; Ogasawara, S.; Fujii, Y.; Yamada, S.; Murata, T.; Uchida, H.; Tahara, H.; Nishioka, Y.; Kato, Y. Chimeric Anti-Human Podoplanin Antibody NZ-12 of Lambda Light Chain Exerts Higher Antibody-Dependent Cellular Cytotoxicity and Complement-Dependent Cytotoxicity Compared with NZ-8 of Kappa Light Chain. *Monoclon Antib Immunodiagn Immunother* **2017**, *36*, 25-29, doi:10.1089/mab.2016.0047.
42. Ito, A.; Ohta, M.; Kato, Y.; Inada, S.; Kato, T.; Nakata, S.; Yatabe, Y.; Goto, M.; Kaneda, N.; Kurita, K.; et al. A Real-Time Near-Infrared Fluorescence Imaging Method for the Detection of Oral Cancers in Mice Using an Indocyanine Green-Labeled Podoplanin Antibody. *Technol Cancer Res Treat* **2018**, *17*, 1533033818767936, doi:10.1177/1533033818767936.
43. Tamura, R.; Oi, R.; Akashi, S.; Kaneko, M.K.; Kato, Y.; Nogi, T. Application of the NZ-1 Fab as a crystallization chaperone for PA tag-inserted target proteins. *Protein Sci* **2019**, *28*, 823-836, doi:10.1002/pro.3580.
44. Shiina, S.; Ohno, M.; Ohka, F.; Kuramitsu, S.; Yamamichi, A.; Kato, A.; Motomura, K.; Tanahashi, K.; Yamamoto, T.; Watanabe, R.; et al. CAR T Cells Targeting Podoplanin Reduce Orthotopic Glioblastomas in Mouse Brains. *Cancer Immunol Res* **2016**, *4*, 259-268, doi:10.1158/2326-6066.Cir-15-0060.
45. Kuwata, T.; Yoneda, K.; Mori, M.; Kanayama, M.; Kuroda, K.; Kaneko, M.K.; Kato, Y.; Tanaka, F. Detection of Circulating Tumor Cells (CTCs) in Malignant Pleural Mesothelioma (MPM) with the "Universal" CTC-Chip and An Anti-Podoplanin Antibody NZ-1.2. *Cells* **2020**, *9*, doi:10.3390/cells9040888.
46. Nishinaga, Y.; Sato, K.; Yasui, H.; Taki, S.; Takahashi, K.; Shimizu, M.; Endo, R.; Koike, C.; Kuramoto, N.; Nakamura, S.; et al. Targeted Phototherapy for Malignant Pleural Mesothelioma: Near-Infrared Photoimmunotherapy Targeting Podoplanin. *Cells* **2020**, *9*, doi:10.3390/cells9041019.
47. Fujii, Y.; Kaneko, M.; Neyazaki, M.; Nogi, T.; Kato, Y.; Takagi, J. PA tag: a versatile protein tagging system using a super high affinity antibody against a dodecapeptide derived from human podoplanin. *Protein Expr Purif* **2014**, *95*, 240-247, doi:10.1016/j.pep.2014.01.009.
48. Kato, Y.; Kaneko, M.K.; Kunita, A.; Ito, H.; Kameyama, A.; Ogasawara, S.; Matsuura, N.; Hasegawa, Y.; Suzuki-Inoue, K.; Inoue, O.; et al. Molecular analysis of the pathophysiological binding of the platelet aggregation-inducing factor podoplanin to the C-type lectin-like receptor CLEC-2. *Cancer Sci* **2008**, *99*, 54-61, doi:10.1111/j.1349-7006.2007.00634.x.
49. Kato, Y.; Vaidyanathan, G.; Kaneko, M.K.; Mishima, K.; Srivastava, N.; Chandramohan, V.; Pegram, C.; Keir, S.T.; Kuan, C.T.; Bigner, D.D.; et al. Evaluation of anti-podoplanin rat monoclonal antibody NZ-1 for targeting malignant gliomas. *Nucl Med Biol* **2010**, *37*, 785-794, doi:10.1016/j.nucmedbio.2010.03.010.
50. Suzuki, H.; Ohishi, T.; Asano, T.; Tanaka, T.; Saito, M.; Mizuno, T.; Yoshikawa, T.; Kawada, M.; Kaneko, M.K.; Kato, Y. Defucosylated mouse-dog chimeric anti-HER2 monoclonal antibody exerts antitumor activities in mouse xenograft models of canine tumors. *Oncol Rep* **2022**, *48*, doi:10.3892/or.2022.8366.
51. Kato, Y. Specific monoclonal antibodies against IDH1/2 mutations as diagnostic tools for gliomas. *Brain Tumor Pathol* **2015**, *32*, 3-11, doi:10.1007/s10014-014-0202-4.
52. Ikota, H.; Nobusawa, S.; Arai, H.; Kato, Y.; Ishizawa, K.; Hirose, T.; Yokoo, H. Evaluation of IDH1 status in diffusely infiltrating gliomas by immunohistochemistry using anti-mutant and wild type IDH1 antibodies. *Brain Tumor Pathol* **2015**, *32*, 237-244, doi:10.1007/s10014-015-0222-8.
53. Kato, Y.; Ohishi, T.; Yamada, S.; Itai, S.; Takei, J.; Sano, M.; Nakamura, T.; Harada, H.; Kawada, M.; Kaneko, M.K. Anti-Human Epidermal Growth Factor Receptor 2 Monoclonal Antibody H2Mab-41 Exerts Antitumor Activity in a Mouse Xenograft Model of Colon Cancer. *Monoclon Antib Immunodiagn Immunother* **2019**, *38*, 157-161, doi:10.1089/mab.2019.0017.
54. Li, G.; Ohishi, T.; Kaneko, M.K.; Takei, J.; Mizuno, T.; Kawada, M.; Saito, M.; Suzuki, H.; Kato, Y. Defucosylated Mouse-Dog Chimeric Anti-EGFR Antibody Exerts Antitumor Activities in Mouse Xenograft Models of Canine Tumors. *Cells* **2021**, *10*, doi:10.3390/cells10123599.
55. Takei, J.; Kaneko, M.K.; Ohishi, T.; Kawada, M.; Harada, H.; Kato, Y. H2Mab-19, an anti-human epidermal growth factor receptor 2 monoclonal antibody exerts antitumor activity in mouse oral cancer xenografts. *Exp Ther Med* **2020**, *20*, 846-853, doi:10.3892/etm.2020.8765.

56. Takei, J.; Ohishi, T.; Kaneko, M.K.; Harada, H.; Kawada, M.; Kato, Y. A defucosylated anti-PD-L1 monoclonal antibody 13-mG2a-f exerts antitumor effects in mouse xenograft models of oral squamous cell carcinoma. *Biochem Biophys Rep* **2020**, *24*, 100801, doi:10.1016/j.bbrep.2020.100801.
57. Tateyama, N.; Asano, T.; Ohishi, T.; Takei, J.; Hosono, H.; Nanamiya, R.; Tanaka, T.; Sano, M.; Saito, M.; Kawada, M.; et al. An Anti-HER2 Monoclonal Antibody H2Mab-41 Exerts Antitumor Activities in Mouse Xenograft Model Using Dog HER2-Overexpressed Cells. *Monoclon Antib Immunodiagn Immunother* **2021**, *40*, 184-190, doi:10.1089/mab.2021.0025.
58. Tateyama, N.; Nanamiya, R.; Ohishi, T.; Takei, J.; Nakamura, T.; Yanaka, M.; Hosono, H.; Saito, M.; Asano, T.; Tanaka, T.; et al. Defucosylated Anti-Epidermal Growth Factor Receptor Monoclonal Antibody 134-mG2a-f Exerts Antitumor Activities in Mouse Xenograft Models of Dog Epidermal Growth Factor Receptor-Overexpressed Cells. *Monoclon Antib Immunodiagn Immunother* **2021**, *40*, 177-183, doi:10.1089/mab.2021.0022.
59. Cardoso, F.; Paluch-Shimon, S.; Senkus, E.; Curigliano, G.; Aapro, M.S.; André, F.; Barrios, C.H.; Bergh, J.; Bhattacharyya, G.S.; Biganzoli, L.; et al. 5th ESO-ESMO international consensus guidelines for advanced breast cancer (ABC 5). *Ann Oncol* **2020**, *31*, 1623-1649, doi:10.1016/j.annonc.2020.09.010.
60. Hao, Y.; Yu, X.; Bai, Y.; McBride, H.J.; Huang, X. Cryo-EM Structure of HER2-trastuzumab-pertuzumab complex. *PLoS One* **2019**, *14*, e0216095, doi:10.1371/journal.pone.0216095.
61. Tateyama, N.; Suzuki, H.; Ohishi, T.; Asano, T.; Tanaka, T.; Mizuno, T.; Yoshikawa, T.; Kawada, M.; Kaneko, M.K.; Kato, Y. Antitumor Activity of an Anti-EGFR/HER2 Bispecific Antibody in a Mouse Xenograft Model of Canine Osteosarcoma. *Pharmaceutics* **2022**, *14*, doi:10.3390/pharmaceutics14112494.
62. Greulich, H.; Kaplan, B.; Mertins, P.; Chen, T.H.; Tanaka, K.E.; Yun, C.H.; Zhang, X.; Lee, S.H.; Cho, J.; Ambrogio, L.; et al. Functional analysis of receptor tyrosine kinase mutations in lung cancer identifies oncogenic extracellular domain mutations of ERBB2. *Proc Natl Acad Sci U S A* **2012**, *109*, 14476-14481, doi:10.1073/pnas.1203201109.
63. Takegawa, N.; Nonagase, Y.; Yonesaka, K.; Sakai, K.; Maenishi, O.; Ogitani, Y.; Tamura, T.; Nishio, K.; Nakagawa, K.; Tsurutani, J. DS-8201a, a new HER2-targeting antibody-drug conjugate incorporating a novel DNA topoisomerase I inhibitor, overcomes HER2-positive gastric cancer T-DM1 resistance. *Int J Cancer* **2017**, *141*, 1682-1689, doi:10.1002/ijc.30870.
64. Modi, S.; Saura, C.; Yamashita, T.; Park, Y.H.; Kim, S.B.; Tamura, K.; Andre, F.; Iwata, H.; Ito, Y.; Tsurutani, J.; et al. Trastuzumab Deruxtecan in Previously Treated HER2-Positive Breast Cancer. *N Engl J Med* **2020**, *382*, 610-621, doi:10.1056/NEJMoa1914510.
65. Li, B.T.; Smit, E.F.; Goto, Y.; Nakagawa, K.; Udagawa, H.; Mazières, J.; Nagasaka, M.; Bazhenova, L.; Saltos, A.N.; Felip, E.; et al. Trastuzumab Deruxtecan in HER2-Mutant Non-Small-Cell Lung Cancer. *N Engl J Med* **2021**, doi:10.1056/NEJMoa2112431.
66. Modi, S.; Saura, C.; Yamashita, T.; Park, Y.H.; Kim, S.B.; Tamura, K.; Andre, F.; Iwata, H.; Ito, Y.; Tsurutani, J.; et al. Trastuzumab Deruxtecan in Previously Treated HER2-Positive Breast Cancer. *N Engl J Med* **2020**, *382*, 610-621, doi:10.1056/NEJMoa1914510.
67. Shitara, K.; Bang, Y.J.; Iwasa, S.; Sugimoto, N.; Ryu, M.H.; Sakai, D.; Chung, H.C.; Kawakami, H.; Yabusaki, H.; Lee, J.; et al. Trastuzumab Deruxtecan in Previously Treated HER2-Positive Gastric Cancer. *N Engl J Med* **2020**, *382*, 2419-2430, doi:10.1056/NEJMoa2004413.
68. Li, B.T.; Smit, E.F.; Goto, Y.; Nakagawa, K.; Udagawa, H.; Mazières, J.; Nagasaka, M.; Bazhenova, L.; Saltos, A.N.; Felip, E.; et al. Trastuzumab Deruxtecan in HER2-Mutant Non-Small-Cell Lung Cancer. *N Engl J Med* **2022**, *386*, 241-251, doi:10.1056/NEJMoa2112431.
69. Modi, S.; Jacot, W.; Yamashita, T.; Sohn, J.; Vidal, M.; Tokunaga, E.; Tsurutani, J.; Ueno, N.T.; Prat, A.; Chae, Y.S.; et al. Trastuzumab Deruxtecan in Previously Treated HER2-Low Advanced Breast Cancer. *N Engl J Med* **2022**, *387*, 9-20, doi:10.1056/NEJMoa2203690.
70. Mercogliano, M.F.; Bruni, S.; Mauro, F.L.; Schillaci, R. Emerging Targeted Therapies for HER2-Positive Breast Cancer. *Cancers (Basel)* **2023**, *15*, doi:10.3390/cancers15071987.
71. Popović, M.; Silovski, T.; Križić, M.; Dedić Plavetić, N. HER2 Low Breast Cancer: A New Subtype or a Trojan for Cytotoxic Drug Delivery? *Int J Mol Sci* **2023**, *24*, doi:10.3390/ijms24098206.
72. Corti, C.; Giugliano, F.; Nicolò, E.; Tarantino, P.; Criscitiello, C.; Curigliano, G. HER2-Low Breast Cancer: a New Subtype? *Curr Treat Options Oncol* **2023**, *24*, 468-478, doi:10.1007/s11864-023-01068-1.
73. Shinkawa, T.; Nakamura, K.; Yamane, N.; Shoji-Hosaka, E.; Kanda, Y.; Sakurada, M.; Uchida, K.; Anazawa, H.; Satoh, M.; Yamasaki, M.; et al. The absence of fucose but not the presence of galactose or bisecting N-acetylglucosamine of human IgG1 complex-type oligosaccharides shows the critical role of enhancing antibody-dependent cellular cytotoxicity. *J Biol Chem* **2003**, *278*, 3466-3473, doi:10.1074/jbc.M210665200.
74. Antoniu, S.A. Mogamulizumab, a humanized mAb against C-C chemokine receptor 4 for the potential treatment of T-cell lymphomas and asthma. *Curr Opin Mol Ther* **2010**, *12*, 770-779.

75. Kato, Y.; Kaneko, M.K. A cancer-specific monoclonal antibody recognizes the aberrantly glycosylated podoplanin. *Sci Rep* **2014**, *4*, 5924, doi:10.1038/srep05924.
76. Kaneko, M.K.; Nakamura, T.; Kunita, A.; Fukayama, M.; Abe, S.; Nishioka, Y.; Yamada, S.; Yanaka, M.; Saidoh, N.; Yoshida, K.; et al. ChLpMab-23: Cancer-Specific Human-Mouse Chimeric Anti-Podoplanin Antibody Exhibits Antitumor Activity via Antibody-Dependent Cellular Cytotoxicity. *Monoclon Antib Immunodiagn Immunother* **2017**, *36*, 104-112, doi:10.1089/mab.2017.0014.
77. Kaneko, M.K.; Yamada, S.; Nakamura, T.; Abe, S.; Nishioka, Y.; Kunita, A.; Fukayama, M.; Fujii, Y.; Ogasawara, S.; Kato, Y. Antitumor activity of chLpMab-2, a human-mouse chimeric cancer-specific antihuman podoplanin antibody, via antibody-dependent cellular cytotoxicity. *Cancer Med* **2017**, *6*, 768-777, doi:10.1002/cam4.1049.
78. Kaneko, M.K.; Ohishi, T.; Kawada, M.; Kato, Y. A cancer-specific anti-podocalyxin monoclonal antibody (60-mG(2a)-f) exerts antitumor effects in mouse xenograft models of pancreatic carcinoma. *Biochem Biophys Rep* **2020**, *24*, 100826, doi:10.1016/j.bbrep.2020.100826.
79. Suzuki, H.; Kaneko, M.K.; Kato, Y. Roles of Podoplanin in Malignant Progression of Tumor. *Cells* **2022**, *11*, doi:10.3390/cells11030575.
80. Ishikawa, A.; Waseda, M.; Ishii, T.; Kaneko, M.K.; Kato, Y.; Kaneko, S. Improved anti-solid tumor response by humanized anti-podoplanin chimeric antigen receptor transduced human cytotoxic T cells in an animal model. *Genes Cells* **2022**, in press, doi:10.1111/gtc.12972.
81. Chalise, L.; Kato, A.; Ohno, M.; Maeda, S.; Yamamichi, A.; Kuramitsu, S.; Shiina, S.; Takahashi, H.; Ozone, S.; Yamaguchi, J.; et al. Efficacy of cancer-specific anti-podoplanin CAR-T cells and oncolytic herpes virus G47Δ combination therapy against glioblastoma. *Molecular Therapy - Oncolytics* **2022**, *26*, 265-274, doi:https://doi.org/10.1016/j.omto.2022.07.006.